

Low Phase Noise, Record-High Power Optical Parametric Oscillator Tunable from 2.7–4.7 μm for Metrology Applications

Vito F. Pecile^{1,2,*}, Michael Leskowschek¹, Norbert Modsching³, Valentin J. Wittwer³, Thomas Südmeyer³, Oliver H. Heckl^{1,*}

¹ University of Vienna, Faculty of Physics, Faculty Center for Nano Structure Research, Christian Doppler Laboratory for Mid-IR Spectroscopy, Boltzmanngasse 5, 1090 Vienna, Austria

² University of Vienna, Vienna Doctoral School in Physics, Boltzmanngasse 5, 1090 Vienna, Austria

³ Laboratoire Temps-Fréquence (LTF), Institut de Physique, Université de Neuchâtel, Avenue de Bellevaux 51, 2000 Neuchâtel, Switzerland

* vito.pecile@univie.ac.at, oliver.heckl@univie.ac.at

Abstract:

Within the domain of optical frequency comb systems operating in the mid-infrared, extensive exploration has been undertaken regarding critical parameters such as stabilization, coherence, or spectral tunability. Despite this, certain essential parameters remain inadequately addressed, particularly concerning the light source prerequisites for advanced spectroscopy techniques operating in the 3–5 μm spectral region. Specifically, the necessity for high simultaneous stability of average power, spectral shape, and temporal properties, alongside requirements for excellent beam quality and high powers of several Watts, emerges for applications like cavity-enhanced Doppler-free saturation spectroscopy. Existing systems fall short of meeting these rigorous criteria. This study delves into the metrology aspects of an optical parametric oscillator system, with a particular emphasis on its suitability for power-hungry metrology applications. Notably, the highest average power reported in the 3–5 μm region, reaching 10.3 W for the idler output at 3.1 μm , is achieved. Additionally, new aspects, like the analysis of idler phase noise and beam quality and the onset of higher order modes are discussed. These findings represent a significant advancement towards the realization of highly-stable, metrology-grade frequency combs in the mid-infrared, thereby facilitating precision spectroscopy techniques previously constrained by light source average powers and quality limitations.

1 Introduction

Recent applications like human breath analysis [1], spectroscopy in the "fingerprint region" [2], or trace-gas sensing [3] have fostered the development of light sources that expand the optical frequency comb (OFC) technology to the mid-infrared (mid-IR). Several different approaches, among them mode-locked quantum cascade lasers (QCLs) [4], or systems based on parametric amplification, like difference frequency generation (DFG) [5, 6, 7, 8], optical parametric amplifiers (OPAs) [9, 10, 11], or optical parametric oscillators (OPOs) [12, 13, 14, 15, 16, 17, 18, 19, 20, 21] have been explored and experienced a huge gain in attention over the past few years.

While many interesting properties of those systems, among them OFC stabilization [16, 18, 19, 20], coherence [6], spectral tunability [13, 20], spectral stability and stabilization [13, 22] or output power stability [5, 13, 22], have already been studied, several vital parameters have not been discussed in sufficient detail or are still completely missing in literature. This becomes particularly evident when looking at the light source requirements of advanced spectroscopy techniques like cavity-enhanced Doppler-free saturation spectroscopy in the of 3–5 μm region: Here, frequency metrology aspects, like a high simultaneous stability of average power, the spectral shape, as well as temporal properties (i.e., the phase noise (PN)) are important, while at the same time excellent beam quality (i.e., low M^2) at high average powers of up to several Watts is demanded [23]. Additionally, the idler spectra should be tunable over a wide range to access different molecular absorption features, and have a narrow bandwidth (BW) on the order of 50–100 nm full width at half maximum (FWHM), to match the reflective band of state-of-the-art low-loss mirrors in the mid-IR [24], which are used in the enhancement cavity.

Comparing these demands with state-of-the-art systems in the 3–5 μm region and their discussed properties, we find that works which focus on the suitability for metrology aspects report only on very low idler powers of only a few 10s of mW [16, 17, 18, 22], which is several orders of magnitude lower than needed. In contrast, works that report on the highest average powers in this spectral region (7.8 W at 3.57 μm for an OPO system [21] and 6.7 W at 2.90 μm for a DFG based system [5]) do not sufficiently discuss metrology aspects, which is however critical to determine the suitability of the light sources for spectroscopy

arXiv:2403.19360v1 [physics.optics] 28 Mar 2024

experiments. Additionally, several properties which are highly relevant for metrology applications, particularly a direct measurement of the idler PN or beam quality, have, to the best of our knowledge, not been discussed at all in literature for comparable systems.

In this work, we explore metrology aspects of an OPO system with very high output powers and discuss the suitability and perspectives of the OPO platform as a light source for power-hungry metrology applications in the mid-IR with a focus on cavity-enhanced Doppler-free saturation spectroscopy. To the best of our knowledge, we present the highest average power in the 3–5 μm region, reaching 10.3 W for the idler output at 3.1 μm . We analyze the PN of both signal and idler beam, and show that we were able to conserve the PN of the OPO pump. The onset of higher order modes (HOM) in the OPO cavity when scaling to high output powers is discussed and we differentiate between fundamental-mode and HOM operation of the OPO while presenting the respective properties as well as their suitability for metrology applications. The beam quality of both signal and idler is analyzed for both fundamental-mode and HOM operation. Additionally, we discuss spectral stability as well as the stability of the output power of the system. Our OPO features a broad wavelength tunable range from 2700–4700 nm, adjustable by translating the fanout-structured poling period of the used periodically-poled LiNbO₃ (PPLN) crystal. Our results enable the realization of highly-stable, metrology-grade OFCs in the mid-IR regime and pave the way for precision spectroscopy techniques which have so far been limited by the available light source average powers and quality by reaching record high idler powers while at the same time ensuring low PN and excellent beam quality.

2 Experimental Setup

2.1 OPO Setup and Pump

A scheme of the OPO setup is shown in **Figure 1**. A more detailed description of the respective optical components is provided in **Table 1**. The OPO is realized as a synchronously-pumped, signal singly-resonant, X-shaped standing-wave cavity. Cavity mirrors (CM) 1-2 are concave and broadband highly-reflective (HR) for the signal and highly transmissive (HT) for pump and idler. They are separated by 260 mm with the nonlinear crystal placed centered inbetween. CM3 is a plane mirror which is HR for the signal and mounted on a translation stage to match the OPO cavity length to the pump repetition rate. CM4 serves as an output coupler (OC) for the signal. The geometrical distances CM13 and CM24 are ~ 462 mm. The nonlinear crystal used is a 5 mm long MgO(5%)-doped PPLN crystal, which is placed in an oven and operated at 70° C. The poling periods are organized in a fanout structure and can be tuned continuously from 25.5–32.5 μm by translating the PPLN normal to the incident beam path. The PPLN coating is optimized for pump and signal transmission, which leads to roughly 10% idler losses at the exiting PPLN interface.

The pump is an inhouse-built mode-locked 125.4 MHz low-noise Yb: fiber oscillator based on a nonlinear amplifying loop mirror (NALM) [25, 26] amplified by a chirped-pulse amplifier (CPA) [27], which delivers 1042 nm centered, 8 nm FWHM, ~ 550 fs pulses at up to 68 W of average power. The FWHM and the pulse duration are optimized to meet the spectral acceptance BW as well as the temporal walk-off length of the 5 mm long PPLN [28]. The pump beam is aligned to the OPO cavity via mirrors (M) 1-2 and mode-matched to the resonant signal beam via lenses (L) 1-2 [29]. The minimal signal waist radius centered inside the PPLN is estimated to be ~ 80 μm using the ray transfer-matrix method for Gaussian beams [30]. This corresponds to a pump beam waist radius of ~ 65 μm , the related M^2 measurement is shown in Section 3.4. At the highest possible pump power of 68 W the pump peak intensity inside the PPLN is calculated as 14.86 GW/cm². This intensity is higher than reported laser-induced damage thresholds for lithium niobate using similar light sources [31], however, we did not observe any laser-induced damage in our crystal. The pump power can be adjusted by rotating half-wave plate (HWP) 1 and thereby changing the polarization-dependent transmission through the thin-film polarizer (TFP). HWP2 is used to create an s-polarized beam to align the pump polarization with the dipole moment of the PPLN. Both the residual pump and generated idler beams get collimated by L3 and subsequently

Table 1: Specifications of all optics used in the setup shown in Figure 1: RoC, radius of curvature; f, focal length; FS, frontside; BS, backside; R, reflectance for unpolarized light; T, transmittance for unpolarized light; Tp, transmittance for p-polarized light; Ts, transmittance for s-polarized light; AoI, angle of incidence. For all CMs, the FS faces towards the resonant signal beam, for all other optics the FS is the side where the pump and/or idler beam make the transition from air to substrate according to their path highlighted in Figure 1. The coatings specified as "UniNE" were custom designed and manufactured by V.J. Wittwer at Université de Neuchâtel. For all other coatings, the specifications of the respective suppliers were used.

Component	RoC/f	Coating	Substrate	Supplier/Part Number
CM1/CM2	-209.1 mm	FS,BS: R > 99.8% 1340–1570 nm AoI = 7°, FS,BS: T > 98% 1018–1064 nm AoI = 7°, FS,BS: T > 90% 2700–5000 nm AoI = 7°	CaF ₂	Substrate: EKSMA Optics 112-5230E Coating: UniNE
CM3	plane	FS: R > 99.5 % 1200–1800 nm	UVFS	Laseroptik 12239
CM4/OC	plane	FS: R = 85% (\pm 3%) 1400–1800 nm, BS: high T 1400–1800 nm	UVFS	Layertec 106828
PPLN	plane	FS,BS: T > 99% 1040 nm, FS,BS: T > 99% 1310–1650 nm, FS,BS: T > 90% 2800–5050 nm	5% MgO LiNbO ₃	HC Photonics 1BKFL5P13250005100050Y002
DM	plane	FS,BS: R > 99.5% 1020–1060 nm AoI = 45°, BS: T > 99.5% 3000–4500 nm AoI = 45°	CaF ₂	Substrate: EKSMA Optics 530-5253; Coating: UniNE
GW	plane	FS,BS: Thorlabs C9 Coating, T \sim 85–95% 1900–6000 nm	Ge	Thorlabs WG91050-C9
L1	75 mm	FS,BS: Thorlabs YAG Coating, T > 99.5% 1020–1060 nm	UVFS	Thorlabs LA4725-YAG
L2	50 mm	same as L1	UVFS	Thorlabs LA4148-YAG
L3	150 mm	FS,BS: Thorlabs E Coating, Total Average T > 98.75% 2000–5000 nm	CaF ₂	Thorlabs LA5012-E
M1/M2	plane	FS: R > 99.9 % 1000–1060 nm	UVFS	EKSMA Optics 042-1030HHR
HWP1/HWP2	plane	FS: T > 99.5 % 1030 nm	UVFS	EKSMA Optics 464-4208
TFP	plane	Total Tp > 98 % 1030 nm AoI = 45°, Tp/Ts > 1000:1	UVFS	EKSMA Optics 420-1248i45HE

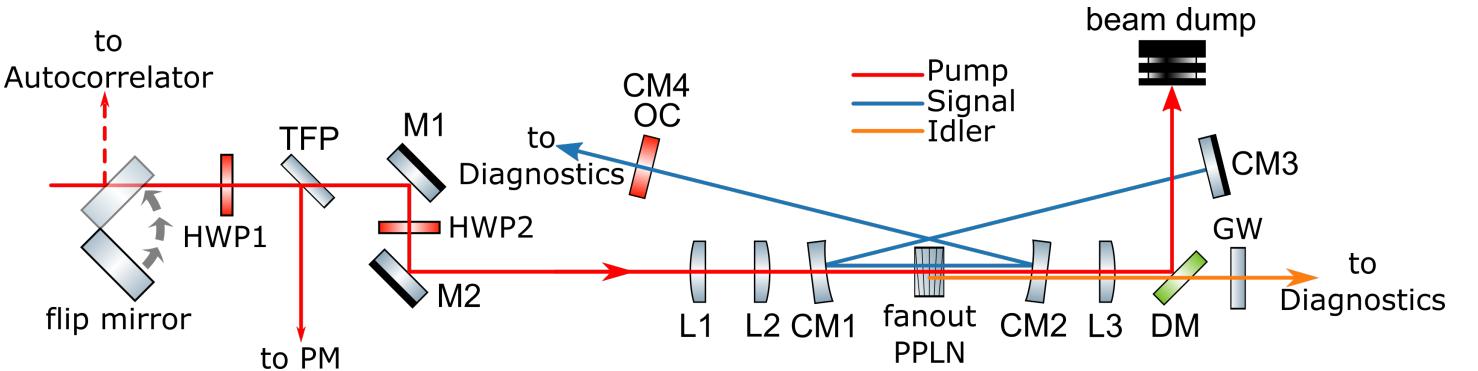


Figure 1: Scheme of the OPO setup: HWP1-2, half-wave plates; TFP, thin-film polarizer; M1-2, mirrors; PM, powermeter; L1-3, lenses; CM1-4, cavity mirrors; OC, 15% output coupler; DM, dichroic mirror; GW, germanium window; PPLN, periodically-poled LiNbO₃ crystal.

separated by a dichroic mirror (DM). The residual pump is then dumped, the idler is transmitted through a germanium window (GW) to be cleaned from any leakage through the DM.

2.2 Measurement Setup

In this work we analyzed the optical spectra, average powers, PN, as well as the beam quality (M^2 and spatial beam profiles) of the pump, signal and idler beams. All spectra of the signal were recorded with a Yokogawa AQ6374 grating-based optical spectrum analyzer (OSA) with a resolution bandwidth (RBW) of 2 nm. The spectra of the idler were measured with a Thorlabs OSA305 Fourier-transform OSA with a RBW of 2.1 nm.

The pump power was measured indirectly with a Thorlabs S425C-L powermeter (PM) by measuring the power of the beam reflected by the TFP and subtracting the measured value from the total power. The power of both signal and idler were directly measured with a Thorlabs S425C PM. The PN of pump and signal as well as all presented RF-traces were obtained with a 5 GHz BW InGaAs photodetector (PD; Thorlabs DET08CL). The PN of the idler was measured with a 1 GHz BW HgCdTe PD (Vigo Photonics UHSM-10.6). A Rohde & Schwarz FSWP-8 was used for PN and RF trace analysis. All PN measurements presented in the script show $\mathcal{L}(f) \equiv S_\phi(f)/2 = S_{SSB}(f)$ where $\mathcal{L}(f)$ is the standard measure of phase instability, $S_\phi(f)$ is the PN power spectral density (PSD), and $S_{SSB}(f)$ is the single sideband (SSB) PSD, following the current IEEE standard definitions [32]. The PN traces presented in this work were measured at a higher harmonic n of the repetition rate to increase the measurement sensitivity with respect to the shot-noise limit and then corrected to receive the PN of the repetition rate by subtracting the term $20 \log_{10}(n)$ from the whole PN trace, as similarly done in Modsching et al. [33]. The pump was measured at $n = 16$, the signal at $n = 19$ and the idler at $n = 8$. The spatial beam profiles were recorded and the M^2 measurement of the pump was performed with a Newport LBP2-HR-VIS2 laser beam profiler, for the signal and idler an Ophir Spiricon Pyrocam IV beam profiling system was used. The M^2 measurements were performed according to ISO 11146-1:2021.

3 Results and Discussion

3.1 Fundamental Mode Operation and Spectral Tuning Range

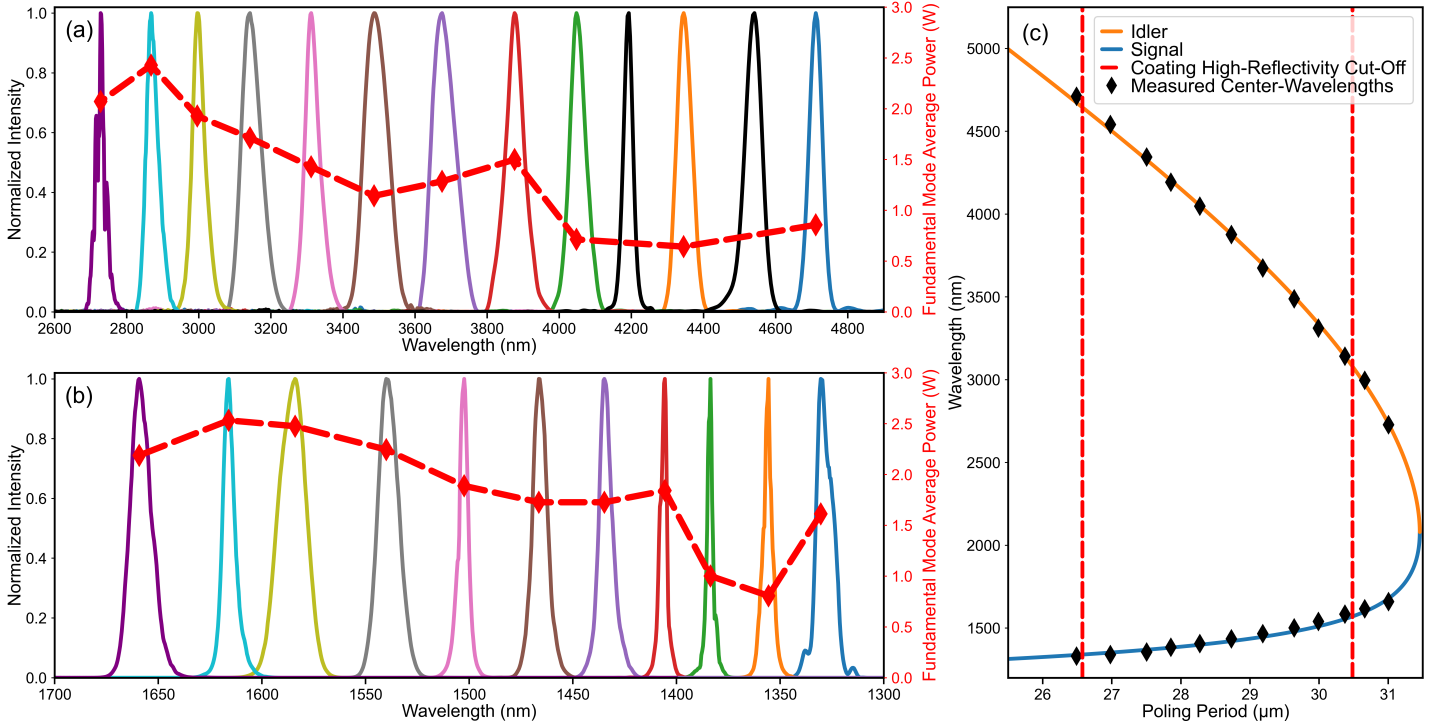


Figure 2: Normalized spectra of the (a) idler and the (b) signal in fundamental-mode operation over the whole supported spectral tuning range. The spectra obtained at the same poling period are color-matched. Note, that the corresponding signal of the two idler spectra shown in black are not presented to omit overcrowding in the signal plot. The features for the idler at ~ 2750 nm (purple) are attributed to CO_2 absorption in air. The red dotted lines in (a) and (b) show the highest achieved average power in fundamental-mode operation prior to the excitation of HOM. The idler powers are corrected for the germanium window losses. (c) Calculated QPM curve for different poling periods of the used PPLN for the idler (orange) and signal (blue). The BW supported by the used coatings in the cavity (for details please refer to Table 1; coating cut-offs shown in dashed red) can be exceeded slightly without significantly higher losses. The center wavelengths of the measured signal-idler-pairs (black diamonds) show good agreement with the theoretical QPM curve.

Measured spectra for the idler and signal in fundamental-mode operation over the whole spectral range

are shown in **Figure 2** (a) and (b), respectively. The obtained average output powers for the signal and idler are depicted in the respective plots on the secondary y-axis. The calculated quasi-phase-matching (QPM) curve and determined center wavelengths of signal and idler are presented in Figure 2 (c). Fundamental-mode operation was ensured by measuring a conservation of the pump PN for the signal and idler beams, as is discussed in greater detail in Section 3.3. We received bell-shaped spectra over the whole spectral range with a FWHM of 45–85 nm for the idler and 5–15 nm for the signal. The OPO threshold was in the range of 300–500 mW for idler wavelengths below 4000 nm and increased gradually for wavelengths larger than 4000 nm, reaching ~ 1800 mW at 4700 nm. The photon-to-photon conversion efficiency (PCE) was calculated to be $\sim 40\%$ for idler wavelengths of 2700–3900 nm. Beyond 4000 nm, 35–10% could be achieved, decreasing with higher wavelengths. These values are similar to PCEs reported for other signal singly-resonant OPO systems operating in the same spectral region, where 35–50% are achieved for wavelengths smaller 4000 nm before gradually dropping down to $\sim 10\%$ for higher idler wavelengths [13, 20]. The decreased performance for higher idler wavelengths is expected, as the OPO process experiences less gain when moving away from degeneracy [11, 34, 35]. Additionally, PPLN crystals show increased absorption above 4000 nm [31].

The highest average power in fundamental-mode operation achieved for the idler was 2.43 W at a wavelength of 2870 nm. The lowest average power was obtained as 0.64 W at 4345 nm. To best of our knowledge, those are the highest average powers reported over the whole tuning range of our system (2700–4700 nm), compared to other wavelength tunable parametric sources operating in the same wavelength regime [13, 20]. In general, the obtained idler powers in fundamental-mode operation become smaller with higher wavelengths. This is explainable with two effects: First, the average powers for higher wavelengths are smaller, as the energy per photon decreases with increasing wavelength. Second, when moving away from degeneracy, the OPO process experiences less gain, as already discussed above.

For the signal, the highest fundamental-mode average power was measured as 2.53 W at 1615 nm, the lowest as 0.81 W at 1355 nm. Here, we see the same trend as for the idler: When moving away from degeneracy, we achieve lower average powers. However, here the difference is smaller compared to the idler: As we move towards shorter wavelengths, the photons carry more energy and higher average powers are achieved even when lower gains are present.

3.2 Higher-Order-Mode Behavior

When the pump power is increased beyond the fundamental-mode limit, HOMs are excited in the OPO cavity. In the following, we discuss the HOM behavior exemplarily for an idler wavelength of 3100 nm. The corresponding power slope is shown in **Figure 3** (e). We achieve 10.3 W idler average power at a pump power of 68 W, which, to the best of our knowledge, is the highest average power in the 3–5 μm region so far reported [5, 21]. The PCE amounts to 45% at maximal pump power, which is slightly higher than the results received for fundamental-mode operation. We also achieve a signal average power of 12.8 W at 1550 nm for maximal pump power, which is among the highest powers reported in that specific wavelength region [21]. The output power stability of the system was recorded and the standard deviation (SD) calculated over 45 min, showing a stability of 0.84% for the idler and 1.04% for the signal (see Figure 3(c), (d), respectively). The used sampling interval was 0.5 s. These results are surprisingly good, as we only see slightly higher instabilities compared to values reported for low-power systems well below 100 mW, which achieved idler stabilities of 0.62% in free-running operation [13] and 0.30% with active cavity length stabilization [22], even though we operate at more than 100 times higher power. The signal and idler powers show a linear slow-term drift over the full measurement time which is attributed to the walk-off of the pump and signal pulses due to cavity length fluctuations. In the presented configuration both the seed oscillator as well as the OPO were free-running, with the OPO being operated in an open lab environment. A further improvement in stability can be expected by applying, e.g., active cavity length stabilization schemes or passive thermal shielding.

The recorded optical spectra at full pump power of the idler and the signal are shown in Figure 3 (a) and (b), respectively. They are significantly more broadband as the fundamental-mode spectra shown in Figure 2 (a) and (b) (the idler expands roughly over 400 nm, the signal almost over 100 nm), featuring sev-

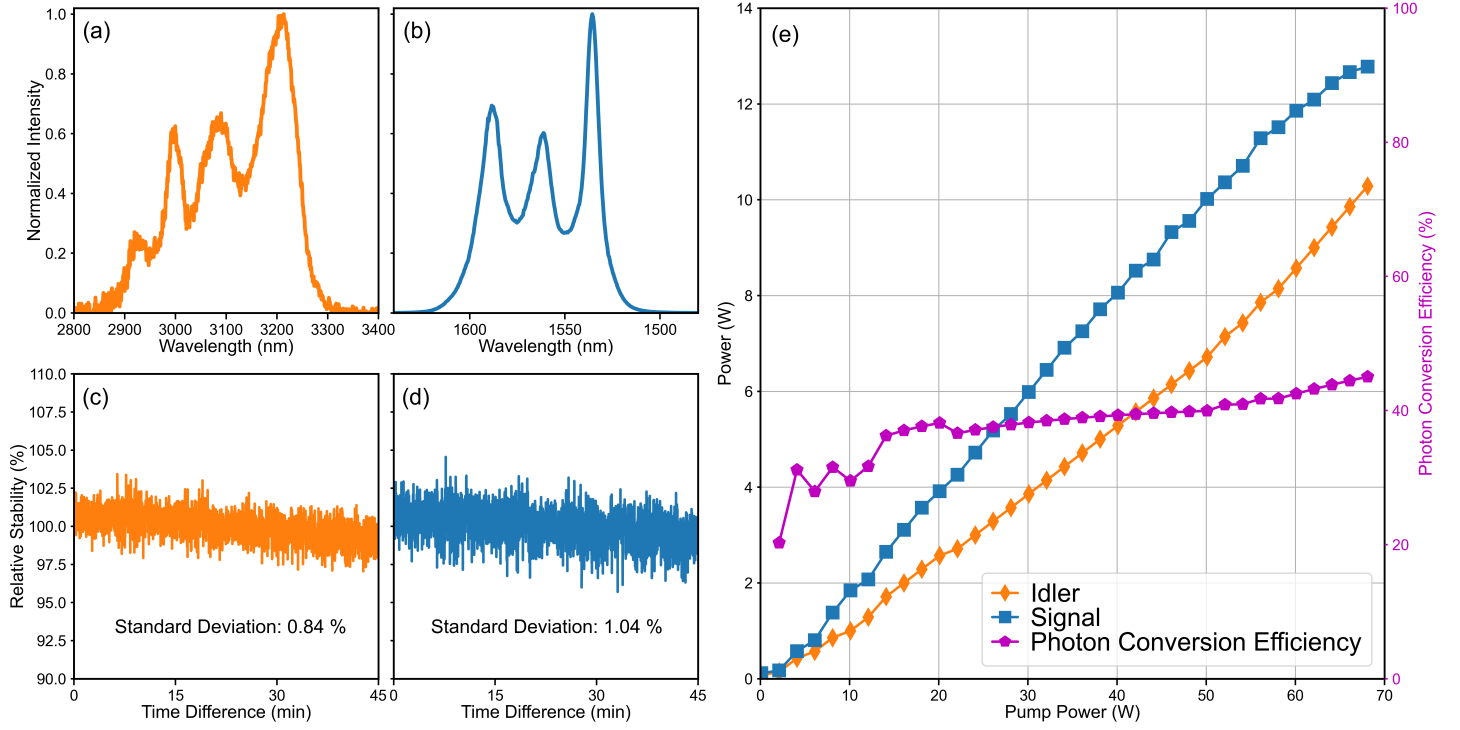


Figure 3: Normalized spectrum of the (a) idler and the (b) signal at full pump power in stable HOM operation. 45 min average power stability measurement of the idler (c) and the signal (d). The single measurement values are normalized to the mean value. The sampling interval was 0.5 s. (e) Pump power slope of signal and idler. The idler power values are corrected for the germanium window transmission losses. The OPO was realigned at 50 W pump power to compensate for thermal effects, which lead to a steeper slope efficiency for the highest pump powers. The slight decrease in slope efficiency for high signal powers is caused by operating the used PM outside of its 10 W maximal power rating, which leads to a decreased response.

eral distinct peaks. For stable operation in the HOM regime a realignment of the OPO cavity right after reaching the desired pump power and again after a thermalization period (usually around 30 min) was critical to achieve stable operation. Without realignment, mode-beating can be observed and both the spectra of signal and idler as well as their respective output powers become instable.

3.3 Phase Noise Analysis

The PN of the repetition rate of pump, signal and idler in fundamental-mode operation is shown in **Figure 4** (a). We see, that the pump PN is conserved over the full range of Fourier frequencies. The here exemplarily presented PN measurements have been performed with the idler set to 3300 nm and the signal to 1580 nm. Both pump and signal PN are limited by photon shot-noise for Fourier frequencies larger 40 kHz. In the case of the idler, PN conservation can only be guaranteed up to ~ 10 kHz, as we are here limited by the intrinsic noise floor of the used PD before reaching shot-noise. However, we can observe a very good agreement of all curves for all Fourier frequencies within their respective measurement limitations.

The changes in PN for HOM onset are shown in Figure 4 (b). The pump PN can not be conserved in this case. The first changes in PN which usually appear in the case of HOM onset are very narrow peaks appearing as additional features in the measured traces. These peaks represent beating between the fundamental mode and HOM due to their different longitudinal mode number [36]. In the here presented traces they can be seen at Fourier frequencies of ~ 8 kHz and ~ 9 MHz. Additionally, broad features in the Fourier frequency range of a few 100 kHz to a few MHz are typical, as shown here for both the signal and idler traces.

Changes in PN could already be observed, when all other diagnostic means used throughout this study would still indicate fundamental-mode operation, i.e., no degradation in beam quality, or change in the

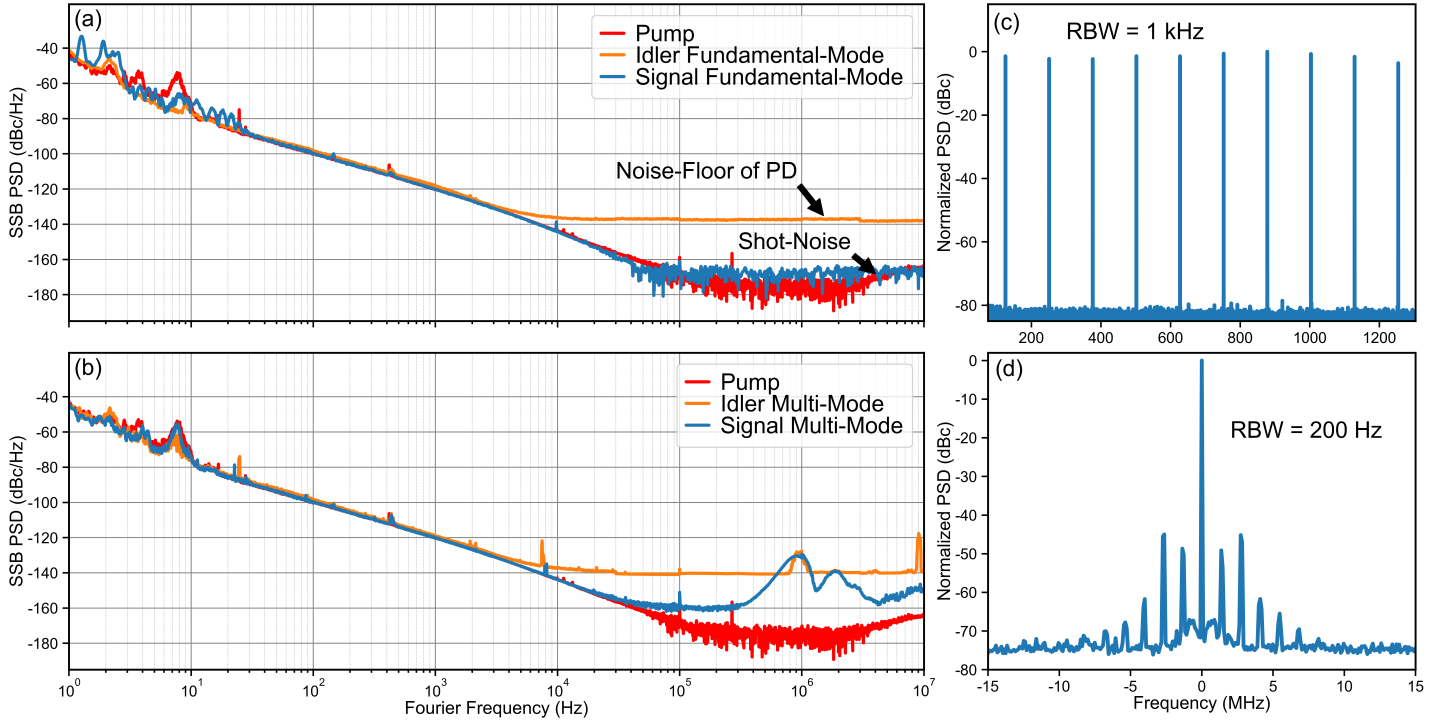


Figure 4: Phase noise analysis of the OPO in fundamental-mode (a) and HOM onset (b) operation. We see, that the PN of the pump is conserved in case of fundamental-mode operation for both signal and idler. The pump and signal measurements are limited by photon shot-noise at high Fourier frequencies, while the idler measurement is limited by the intrinsic noise of the used PD. In the case of HOM operation, we see additional features appearing for both signal and idler. (c) RF spectrum of the signal in the case of HOM onset. Even though distortions are already clearly visible in the PN (the trace corresponds to the data presented in (b)), no modulations can be seen in the RF trace. (d) Zoom into the fundamental harmonic of the repetition rate for the signal in the case of stable HOM operation at a pump power significantly above the HOM threshold.

optical spectrum as well as the RF spectrum of the PDs could be noticed. For example, in Figure 4(c) we show the RF spectrum of the signal that corresponds to the PN trace presented in (b), resembling a clean Dirac-comb up to a SNR of >80 dB, where no modulations or any other perturbations can yet be observed. Only when the pump power is further increased beyond the HOM onset threshold, the HOM behavior of the OPO can also be directly observed in the RF traces, as these modulations become clearly visible, which we show exemplarily for the fundamental harmonic of the signal in Figure 4(d).

Summarizing, we could show that signal and idler PN are preserved in the case of fundamental-mode operation of the OPO cavity. A HOM onset can already be detected by PN measurements before any instability in the optical spectrum or modulations in the RF spectrum as well as a beam quality degradation can be observed. PN measurements therefore are identified as the most sensitive means to assess fundamental-mode stability of an OPO cavity and detect HOM onset early on. Additionally, we could show that signal and idler show the same PN performance. This enables for a prediction of the temporal properties of the idler based solely on a characterization of the near-infrared signal beam, where detectors are cheap and available off-the-shelf, while mid-IR PDs are still scarcely available and expensive.

3.4 Beam Quality Measurements

M^2 measurements for idler and signal in fundamental-mode operation are shown in **Figure 5** (a) and (b), respectively. The M^2 measurement of the pump beam is shown in Figure 5(c). The pump measurement was performed between CM1 and CM2 (with removed PPLN) and therefore resembles the OPO cavity mode-matching configuration used in our setup. The corresponding collimated beam profiles are shown in Figure 5(d), (e) and (f). The here discussed measurements were performed at an idler wavelength of 3300 nm and a signal wavelength of 1500 nm.

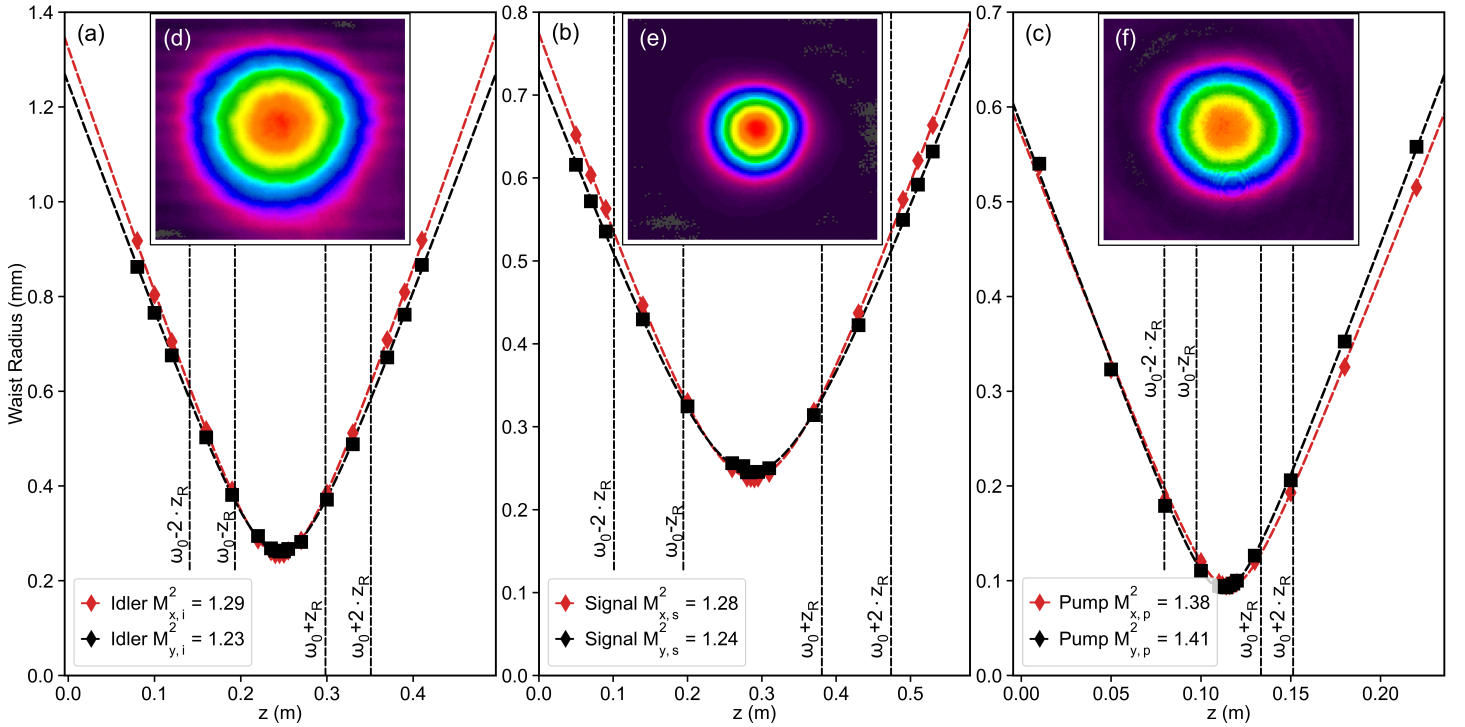


Figure 5: Fundamental-mode M^2 measurement for (a) idler, (b) signal and (c) pump. The pump measurement was performed between CM1 and CM2 (with removed PPLN) and therefore corresponds to the mode-matching configuration used in the here presented work. The indices x and y refer to the horizontal and vertical planes, respectively, i , s and p refer to the idler, signal and pump beams. The distances of one, respectively two Rayleigh lengths (z_R) from the minimal waist positions (ω_0) are shown as black dashed lines. Collimated beam profiles of fundamental-mode idler (d), signal (e) and pump (f). Please note, that the "fringes" seen in inset (d) are caused by the chopper of the used beam profiler (Pyrocam IV) and are a measurement artefact.

For the idler we received values of $M_{x,i}^2 = 1.29$ in the horizontal and $M_{y,i}^2 = 1.23$ in the vertical plane. For the signal we obtained $M_{x,s}^2 = 1.28$ and $M_{y,s}^2 = 1.24$, which shows very good agreement with the values retrieved for the idler. In both cases, the beams have slightly lower M^2 values in the vertical plane. This can be explained by the horizontal tilt of CM1 and CM2 relative to the resonant signal beam wavefront and the thereby introduced beam ellipticity, which is also predicted by calculations using the ray transfer-matrix method for the sagittal and tangential planes separately [30].

For the pump beam we received values of $M_{x,p}^2 = 1.38$ and $M_{y,p}^2 = 1.41$. We see, that both signal and idler beam show a better beam quality, i.e., a lower M^2 value than the incident pump beam. Additionally, the slight astigmatism of the pump beam (see Figure 5(c)) can not be observed for both signal and idler. We attribute this to the nature of the parametric process itself: Areas with high intensity contribute stronger to nonlinear conversion and therefore only parts of the pump beam close to the center contribute, leading to "cleaned" signal and idler beams.

4 Conclusion and Outlook

A high-power low-PN OPO system with a focus on its suitability for power-hungry metrology applications was investigated. We could show, that parametric systems can reach very high idler output powers, achieving the record-high average power of 10.3 W at 3100 nm with an excellent power stability of 0.84% (SD). We discussed that very high output powers in OPOs lead to HOM onset, differentiated between fundamental-mode and HOM behavior of the OPO, and highlighted the different properties of both operational regimes. Fundamental-mode operation, which is critical for cavity-enhanced spectroscopy applications, was achieved for up to 2.43 W of average power at 2870 nm reporting, to the best of our knowledge, the highest average powers over the whole tuning range of our system (2700–4700 nm), compared

to other wavelength tunable parametric sources operating in the same wavelength regime. Additionally, we have shown that we were able to conserve the low PN of the pump beam and achieve excellent beam quality ($M^2 < 1.3$) while maintaining narrow spectral widths of the idler beam. To study the suitability of OPOs as platform for high-power mid-IR metrology applications, we investigated several parameters, which have not been reported on before in literature. Examples are a direct measurement of the PN of the mid-IR idler beam as well as its beam quality aspects and interconnections between the signal and idler beam properties. In our here presented work we could also identify PN measurements as the most sensitive diagnostic means to assess fundamental-mode stability and thereby as critical to identify HOM onset early on.

For future systems, we suspect that metrology-grade mid-IR OFCs based on OPOs (i.e. systems that can provide a high simultaneous stability of average power and spectral shape, as well as a low M^2 value and low phase noise) with even higher output power could be achieved by increasing the cavity OC rate and thereby shifting the HOM onset to higher powers. This approach has been successfully implemented by Südmeyer et al., who used very high OC rates of $\sim 96\%$ in combination with a very long, high-gain nonlinear crystal [21]. However, for very high idler average powers in the 10 W regime or beyond, a combination of an OPO system with a subsequent OPA amplification stage seems to be a more promising approach. This has already been shown for low-power mid-IR systems [13]. This way the necessity of very high gain can be avoided, which is known to compromise beam quality [21, 37] and low M^2 values can be maintained even for very high powers.

Summarizing, we presented a highly-stable, low phase noise, metrology-grade OPO system with record-high powers in the 3–5 μm wavelength regime, thereby facilitating advanced metrology and spectroscopy applications previously constrained by power limitations and insufficient light source stability [23].

Acknowledgements

This research was funded in whole or in part by the Austrian Science Fund (FWF) [DOI: 10.55776/P36040 and 10.55776/F1004]. For open access purposes, the author has applied a CC BY public copyright license to any author accepted manuscript version arising from this submission. The financial support by the Austrian Federal Ministry for Digital and Economic Affairs, the National Foundation for Research, Technology and Development and the Christian Doppler Research Association is gratefully acknowledged. The LTF would like to acknowledge its funding: Schweizerischer Nationalfonds zur Förderung der Wissenschaftlichen Forschung (SNSF) (206021_198176 and 206021_170772).

Conflict of Interest

Vito F. Pecile, Michael Leskowschek and Oliver H. Heckl receive funding from Thorlabs Inc.

Data Availability Statement

Data underlying the results presented in this paper are not publicly available at this time but may be obtained from the authors upon reasonable request.

References

- [1] M. Metsälä, *Journal of Breath Research* **2018**, *12*, 2 027104.
- [2] P. B. Changala, M. L. Weichman, K. F. Lee, M. E. Fermann, J. Ye, *Science* **2019**, *363*, 6422 49.
- [3] A. Foltynowicz, P. Masłowski, A. J. Fleisher, B. J. Bjork, J. Ye, *Applied Physics B* **2013**, *110*, 2 163.
- [4] A. Hugi, G. Villares, S. Blaser, H. C. Liu, J. Faist, *Nature* **2012**, *492*, 7428 229.
- [5] A. Catanese, J. Rutledge, M. Silfies, X. Li, H. Timmers, A. S. Kowligy, A. Lind, S. A. Diddams, T. K. Allison, *Optics Letters* **2019**, *45*, 5 1248.
- [6] D. L. Maser, G. Ycas, W. I. Depetri, F. C. Cruz, S. A. Diddams, *Applied Physics B* **2017**, *123*, 5 1.

- [7] C. Hu, W. Yue, T. Chen, P. Jiang, B. Wu, Y. Shen, *Applied Optics* **2017**, *56*, 6 1574.
- [8] R. T. Murray, T. H. Runcorn, E. J. R. Kelleher, J. R. Taylor, *Optics Letters* **2016**, *41*, 11 2446.
- [9] T. Kanai, Y. Lee, M. Seo, D. E. Kim, *Journal of the Optical Society of America B* **2019**, *36*, 9 2407.
- [10] C. Manzoni, G. Cerullo, *Journal of Optics* **2016**, *18*, 10 103501.
- [11] G. Cerullo, S. D. Silvestri, *Review of Scientific Instruments* **2003**, *74*, 1 1.
- [12] C. P. Bauer, S. L. Camenzind, J. Pupeikis, B. Willenberg, C. R. Phillips, U. Keller, *Optics Express* **2022**, *30*, 11 19904.
- [13] M. Nägele, T. Steinle, F. Mörz, H. Linnenbank, A. Steinmann, H. Giessen, *Optics Express* **2020**, *28*, 17 25000.
- [14] N. Jornod, V. J. Wittwer, M. Gaponenko, M. Hoffmann, N. Hempler, G. P. A. Malcolm, G. T. Maker, T. Südmeyer, *Optics Express* **2017**, *25*, 23 28983.
- [15] N. Coluccelli, D. Viola, V. Kumar, A. Perri, M. Marangoni, G. Cerullo, D. Polli, *Optics Letters* **2017**, *42*, 21 4545.
- [16] K. Balskus, S. Schilt, V. J. Wittwer, P. Brochard, T. Ploetzing, N. Jornod, R. A. McCracken, Z. Zhang, A. Bartels, D. Reid, T. Südmeyer, *Optics Express* **2016**, *24*, 8 8370.
- [17] K. Balskus, Z. Zhang, R. A. McCracken, D. T. Reid, *Optics Letters* **2015**, *40*, 17 4178.
- [18] K. F. Lee, N. Granzow, M. A. Schmidt, W. Chang, L. Wang, Q. Coulombier, J. Troles, N. Leindecker, K. L. Vodopyanov, P. G. Schunemann, M. E. Fermann, P. S. J. Russell, I. Hartl, *Optics Letters* **2014**, *39*, 7 2056.
- [19] T. I. Ferreira, J. Sun, D. T. Reid, *Optics Express* **2011**, *19*, 24 24159.
- [20] F. Adler, K. C. Cossel, M. J. Thorpe, I. Hartl, M. E. Fermann, J. Ye, *Optics Letters* **2009**, *34*, 9 1330.
- [21] T. Südmeyer, E. Innerhofer, F. Brunner, R. Paschotta, T. Usami, H. Ito, S. Kurimura, K. Kitamura, D. C. Hanna, U. Keller, *Optics Letters* **2004**, *29*, 10 1111.
- [22] M. Vainio, L. Halonen, *Optics Letters* **2017**, *42*, 14 2722.
- [23] V. Shumakova, O. H. Heckl, *APL Photonics* **2024**, *9*, 1 010803.
- [24] G.-W. Truong, L. W. Perner, D. M. Bailey, G. Winkler, S. B. Cataño-Lopez, V. J. Wittwer, T. Südmeyer, C. Nguyen, D. Follman, A. J. Fleisher, O. H. Heckl, G. D. Cole, *Nature Communications* **2023**, *14*, 1 7846.
- [25] A. S. Mayer, W. Grosinger, J. Fellingner, G. Winkler, L. W. Perner, S. Droste, S. H. Salman, C. Li, C. M. Heyl, I. Hartl, O. H. Heckl, *Optics Express* **2020**, *28*, 13 18946.
- [26] V. F. Pecile, A. S. Mayer, J. K. C. Ballentin, O. H. Heckl, *Optics Express* **2023**, *31*, 22 36824.
- [27] V. Shumakova, V. F. Pecile, J. Fellingner, M. Leskowschek, P. E. C. Aldia, A. S. Mayer, L. W. Perner, S. Salman, M. Fan, P. Balla, S. Schilt, C. M. Heyl, I. Hartl, G. Porat, O. H. Heckl, *Photonics Research* **2022**, *10*, 10 2309.
- [28] V. Ramaiah-Badarla, Doctoral Thesis, Institut de Ciències Fotòniques, Universitat Politècnica de Catalunya, **2014**.
- [29] H. Baker, *Optica Acta: International Journal of Optics* **1980**, *27*, 7 897.

- [30] H. Kogelnik, T. Li, *Applied Optics* **1966**, *5*, 10 1550.
- [31] D. N. Nikogosyan, *Nonlinear Optical Crystals: A Complete Survey*, Springer-Verlag, New York, **2005**.
- [32] IEEE, IEEE Standard Definitions of Physical Quantities for Fundamental Frequency and Time Metrology—Random Instabilities, **2009**.
- [33] N. Modsching, J. Drs, P. Brochard, J. Fischer, S. Schilt, V. J. Wittwer, T. Südmeyer, *Optics Express* **2021**, *29*, 10 15104.
- [34] S. D. Butterworth, M. J. McCarthy, D. C. Hanna, *Optics Letters* **1993**, *18*, 17 1429.
- [35] O. H. Heckl, B. J. Bjork, G. Winkler, P. Bryan Changala, B. Spaun, G. Porat, T. Q. Bui, K. F. Lee, J. Jiang, M. E. Fermann, P. G. Schunemann, J. Ye, *Optics Letters* **2016**, *41*, 22 5405.
- [36] D.-H. Lee, Y. Yoon, B. Kim, J. Lee, Y. Yoo, J. Hahn, *Applied Physics B: Lasers and Optics* **2002**, *74*, 4-5 435.
- [37] G. Arisholm, R. Paschotta, T. Südmeyer, *Journal of the Optical Society of America B* **2004**, *21*, 3 578.